Prediction of Two-Phase Flowfield in Ram Combustors

D. Albagli* and Y. Levy†
Technion, Haifa, Israel

The basic mixing phenomena in a ram combustor are investigated through implementation of an adequate physical model and adoption of a numerical procedure for the solution of the equations representing the flowfield. The proposed physical model is able to predict the flowfield of particle-laden, chemically inert, confined, coaxial turbulent flows. The particulate phase is treated as a continuum that is in dynamic and thermal nonequilibrium with the host fluid. The resulting set of Eulerian conservation equations are numerically solved by means of a modified version of the TEACH-T computer code, which has shown satisfactory convergence characteristics for the cases investigated. Two numerical simulations are performed. The first one, representing low-speed cold flow of confined jets, is the counterpart of an experimental study for the verification of the physical model and its numerical solution. The second simulation adopts the assessed operating conditions of a ram combustor in sustained flight at sea level. Profiles of primitive flow variables obtained from the simulations display a good quantitative agreement with the experimental results in the first case and indicate the mixing performance of a relatively simple ram combustor geometry in the second case.

Nomenclature

A = sectional coalescence/fragmentation coefficient
B,C = sectional vaporization coefficient (source and sink, respectively)
c = specific heat
d = diameter
$\boldsymbol{F}$ = interphase drag force per unit volume
G = turbulence production term
h = convective heat-transfer coefficient
k = turbulence kinetic energy
L = latent heat of vaporization
N = number concentration
Nu = Nusselt number
P = pressure
Q = interphase heat transfer per unit volume
r = radial coordinate
R = gas constant
Re = Reynolds number
S = source term
T = temperature
V = control volume
V = velocity
W = molecular weight
x = abscissa
y = ordinate
Y = specie mass fraction
z = axial coordinate
α = dispersed phase volume fraction
α = outer flow inclination
β = inner flow spread angle
Γ = transport coefficient
γ = specific heat ratio
δ = Kronecker delta
ϵ = turbulence kinetic energy dissipation rate
κ = von Kármán constant
μ = dynamic viscosity
ρ = density; concentration
σ = Prandtl or Schmidt number
τ = shear stress
ϕ = any scalar variable
∇ = operator $\partial/\partial x_i$

Superscripts

$(^{*})$ = absolute
$(\dot{})$ = derivative with respect to time
$(')$ = fluctuating component
$(\bar{})$ = time averaged
$(\tilde{})$ = Favre-averaged

Subscripts

D = drag
g = gaseous phase
H = related to Prandtl number
i = directional component, ith specie
j = directional component
k = directional component, kth particulate phase
l = laminar
P = constant pressure
p = particulate phase
t = turbulent
V = constant volume

Introduction

FUTURE requirements for air-breathing supersonic missiles impose the development of advanced propulsion systems. The ram rocket is considered one of the most promising concepts in this field. In such a system, fuel-rich, metallized solid propellants are burned in a primary combustion chamber. The primary reaction products containing partly unreacted gaseous fuels and metal particles expand through a primary nozzle into a ram combustor, where they mix and subsequently react with secondary ram air and are exhausted through a secondary nozzle (see Fig. 1).

The two-phase flowfield in ram combustors determines the mixing between the fuel-rich primary exhaust and the secondary ram air, which significantly affects the secondary combustion efficiency. The objective of this study is to assess

Received Aug. 15, 1988; revision received Feb. 10, 1989.

*Graduate Student, Faculty of Aerospace Engineering.
†Senior Lecturer, Faculty of Aerospace Engineering. Member AIAA.

the governing equations of the two-phase flowfield and to obtain their numerical solution in a basic ram combustor configuration.

The ability to deal with the complex flowfield in a ram combustor environment requires rigorous knowledge of a number of physical and chemical processes, including turbulent mixing of the gas generator exhaust with the ram air, recirculating flow, finite-rate chemical kinetics of the gaseous fuels, and particulate fuel ignition and combustion.

Although the first operational ram rocket concept was introduced over 30 years ago, systematic theoretical and experimental investigations began to appear in the unclassified literature only in the early 1970's. The development of new measurement techniques and the enhancement of the computational capabilities, together with the growing interest in this field, led to a somewhat more liberal publication policy, enabling more efficient communication among research staff from different backgrounds.

Studies on ram combuster geometry and performance were published by a number of authors, e.g., Gutmark and Schadow,[10] Schadow et al.,[21-24] Smoot et al.,[26,27] Miller et al.,[16] Choudhury,[4] Zetterström et al.,[38] Streby,[29] Tsujikado,[33] Ishikawa,[12] and Stull et al.[30] These works range from cold-flow water-tunnel simulations to combustion characteristics of particle-laden flows, leading to certain basic conclusions:

1) Nonparallel injection of the secondary air enhances mixing, and further enhancement can be obtained by increasing the number of the inlet ports and injection angle.

2) Fuel injector modifications can be effective in widening the stable combustion zone, especially on the fuel-rich side.

3) Both the combustion efficiency and the stability performance are improved by increasing pressure and inlet temperature and by reducing combustor Mach number.

4) The combustion efficiency of metal particles is strongly related to their ignition and multiphase mixing processes in the combustor.

Theoretical studies on confined jets, leading to the basic ram combustor configuration, were carried out by Curtet,[5] Chigier and Beér,[3] Peters et al.,[18] Ghia et al.,[8] Tufts and Smoot,[34] and Razinsky and Brighton.[20] Most of these analyses are based on the boundary-layer approach, often revealing good agreement with experimental data and showing the predominance of the viscous effects in ducted mixing systems.

The incorporation of the particulate phase in such flowfields comprising all types of interaction with the host phase has not as yet been achieved despite the attempts of Migdal and Agosta,[15] Genovese et al.,[7] and DiGiacinto et al.,[6] which preclude certain interphase coupling effects.

Considering the difficulties of dealing with a multitude of coupled mechanisms involved in secondary combustion, it may be concluded that substantial progress toward the prediction of such flowfields has been achieved in recent years. Nevertheless, the models proposed so far suffer from 1) oversimplifying assumptions, such as dynamic and/or thermal equilibrium of the multiphase mixture, and 2) lack of available, quantitative experimental data.

In view of the need for further understanding of the flowfield in ram combustors, the objectives of the present study were determined as the assessment of the conservation equations for two-dimensional, axisymmetric, turbulent, dynamically and thermally coupled two-phase flow of confined coaxial jets (simulating the basic ram combustor configuration), and the numerical solution of the elliptic flowfield.

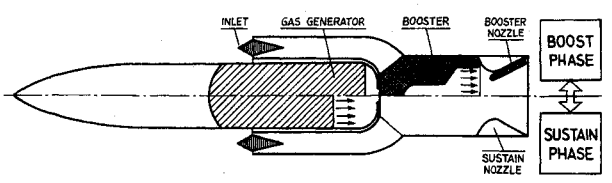

Fig. 1 A typical ram rocket concept.

Physical Model

Basic Assumptions

The physical model implemented in this study predicts the mixing characteristics of particle-laden, confined, coaxial, turbulent jets with coupled mass transport, dynamic and thermal nonequilibrium effects in a simulated ram combustor. The equations governing the flow of both gas and particle phases are assessed according to the Eulerian approach. Effects of chemical reactions are not yet considered in this work.

The major assumptions used in the development of the model are: 1) steady-state flow conditions for all phases; 2) nonreactive, two-component, thermally and calorically perfect, ideal gas phase; 3) uniform, spherical particle base treated as a continuum; 4) k-ϵ isotropic turbulent transport model, excluding particulate phase effects; 5) no Brownian or thermal diffusion of particles; 6) no radiative heat transfer; and 7) no gravity effects.

Governing Equations

Gas Phase Equations

Continuity:

$$\nabla \cdot (\rho_g V_g) = \sum_k \dot{S}_{gk} \tag{1}$$

ith specie:

$$\rho_g (V_g \cdot \nabla) Y_i = \nabla \cdot [(\mu_g/\sigma_i) \nabla Y_i] \tag{2}$$

Momentum:

$$\rho_g (V_g \cdot \nabla) V_g = -\nabla P + \nabla[\nabla \cdot (\mu_g V_g)] - K_M \sum_k F_{pk} - \sum_k (V_g - V_{pk}) \dot{S}_{gk} \tag{3}$$

Thermal energy:

$$\rho_g c_{Pg} (V_g \cdot \nabla) T_g = \nabla \cdot \left(\frac{\mu_g c_{Pg}}{\sigma_H} \nabla T_g \right) + (V_g \cdot \nabla) P - \sum_k \dot{Q}_{pk} - \sum_k |V_g \cdot F_{pk}| - \sum_k L_k \dot{S}_{gk} - \sum_k c_{Pg} (T_g - T_{pk}) \dot{S}_{gk} \tag{4}$$

Turbulence kinetic energy:

$$\rho_g (V_g \cdot \nabla) k = \nabla \cdot [(\mu_g/\sigma_k) \nabla k] + \dot{S}_k \tag{5}$$

Turbulence kinetic energy dissipation rate:

$$\rho_g (V_g \cdot \nabla) \epsilon = \nabla \cdot [(\mu_g/\sigma_\epsilon) \nabla \epsilon] + \dot{S}_\epsilon \tag{6}$$

Particulate Phase Equations

Continuity:

$$\nabla \cdot (\rho_{pk} V_{pk}) = \dot{S}_{pk} \tag{7}$$

Momentum:

$$\rho_{pk} (V_{pk} \cdot \nabla) V_{pk} = \nabla\{\nabla \cdot [(\mu_g/\sigma_{pk}) V_{pk}]\} + F_{pk} + (V_g - V_{pk}) \dot{S}_{gk} + (V_{pk+1} - V_{pk}) B_k \rho_{pk+1} \tag{8}$$

Thermal energy:

$$\rho_{pk} c_{Vpk}(V_{pk} \cdot \nabla)T_{pk} = \nabla \cdot [(\mu_g c_{Vpk}/\sigma_{pHk}) \nabla T_{pk}] + \dot{Q}_{pk} + L_k \dot{S}_{gk} + c_{Vpk}(T_{pk+1} - T_{pk})B_k \rho_{pk+1} \quad (9)$$

Auxiliary Relations

Under the assumption of ideal gas conditions, the equation of state establishes the relationship between the pressure P, gas temperature T_g, and gas density ρ_g,

$$P = \rho_g R_g T_g \quad (10)$$

R_g is the gas constant that can be evaluated from the universal gas constant R_0, the mass fractions of gaseous ingredients Y_i, and their molecular weights W_i,

$$R_g = \sum_i (Y_i/W_i)R_0 \quad (11)$$

The relation between the gaseous phase partial density ρ_g and the gaseous phase absolute density $\hat{\rho}_g$ is

$$\rho_g = \left(1 - \sum_k \alpha_{pk}\right)\hat{\rho}_g \quad (12)$$

α_{pk} being the volume fraction of kth particulate phase in the control volume, namely,

$$\alpha_{pk} = V_{pk}/V \quad (13)$$

Equation (1) describes the conservation of mass within the gaseous phase, i.e., the divergence of the gaseous mass flux vector $\rho_g V_g$ must be equivalent to the total gaseous phase mass production per unit volume, $\Sigma_k \dot{S}_{gk}$, due to the mass transfer from particulate phases. This source term can be related to a combined condensation/vaporization/volume chemical reaction rate E_k to yield

$$\dot{S}_{gk} = \frac{1}{\pi d_{pk}^2} E_k \rho_{pk} \quad (14)$$

where

$$E_k = \dot{d}_{pk}^2 = -\frac{\dot{m}_{pk}}{\pi d_{pk} \rho_{pk}} \quad (15)$$

is evaluated empirically.[36]

Equation (2) is related to the conservation of gaseous species. The source term referring to chemical reactions is omitted in accordance with the model assumptions. The term μ_g is the effective viscosity of the gaseous phase and σ_i represents the Schmidt number of turbulent diffusion for the ith specie, for which various correlations are established.[31]

The first and second terms in the right-hand side of the gaseous phase momentum equation (3) represent the pressure and shear forces applied per unit volume, respectively. The third term is the total drag force exerted on the gas by the particulate phase per unit volume, which can be expressed as

$$F_{pk} = N_{pk} \frac{\pi}{4} d_{pk}^2 C_{Dk} \frac{1}{2} \rho_g |V_g - V_{pk}|(V_g - V_{pk}) \quad (16)$$

and is reduced to the form

$$F_{pk} = \frac{18}{d_{pk}^2} \frac{\rho_{pk}}{\hat{\rho}_{pk}} \mu_g (1 + 0.15 Re_{pk}^{0.687})(V_g - V_{pk}) \quad (17)$$

by implementing the widely used drag coefficient expression[35]

$$C_{Dk} = \frac{24}{Re_{pk}}(1 + 0.15 Re_{pk}^{0.687}) \quad (18)$$

The particle phase concentration ρ_{pk} is the absolute mass of the particles per unit volume, which is calculated from

$$\rho_{pk} = N_{pk} \frac{\pi d_{pk}^3}{6} \hat{\rho}_{pk} \quad (19)$$

whereas N_{pk} denotes the number concentration of the kth particulate phase.

The relative (slip) Reynolds number is defined as

$$Re_{pk} = \frac{\rho_g d_{pk} |V_g - V_{pk}|}{\mu_g} \quad (20)$$

The particulate phase is treated as a true continuum in the model. This implies that a cloud of particles is able to transfer its momentum to the gas in the same way that the gas imparts its momentum to the particles. However, if the particle cloud is to exert a sufficient drag on the gas, the interparticle spacing must be smaller than the diameter plus twice the boundary-layer thickness on the sphere; otherwise, the gas acts as a freestream, with the kinetic energy of particles dissipated completely in their own wakes. To account for this situation, a momentum transfer effectiveness K_M is introduced, such that $K_M = 1$ for the case when particles are accelerated by the gas and $K_M < 1$ when particles are decelerated by it.[28]

The fourth term on the right-hand side of Eq. (3) represents the momentum contribution of the gaseous phase production term (mass transfer from particulate phases) due to interphase velocity lag.

Equation (4) sets the thermal energy balance for the gaseous phase. In general, the temperature of a moving fluid element changes because of heat conduction/radiation, expansion effects, viscous heating, interphase heat/work transfer, and phase change/chemical reaction sources. Radiative heat transfer is not taken into account in this study. An additional effect of the lower order, the viscous dissipation term, is omitted.[2] The first term on the right-hand side of Eq. (4) represents the diffusion of heat by conduction. c_{Pg} is the specific heat of the gaseous phase at constant pressure, σ_H the effective Prandtl number, and T_g the gas temperature. The second term refers to the reversible rate of thermal energy increase per unit volume caused by compression. The third term is the total convective heat transfer from particulate phases per unit volume, which can be written as

$$\dot{Q}_{pk} = N_{pk} \pi d_{pk}^2 h_{pk}(T_g - T_{pk}) \quad (21)$$

which takes the form of

$$\dot{Q}_{pk} = \frac{6}{d_{pk}^2} \frac{\rho_{pk}}{\hat{\rho}_{pk}} \mu_g c_{Pg} \left(\frac{2 + 0.6 Pr^{\frac{1}{3}} Re_{pk}^{\frac{1}{2}}}{Pr}\right)(T_g - T_{pk}) \quad (22)$$

by making use of the relation[14]

$$Nu_{pk} = 2 + 0.6 Pr^{\frac{1}{3}} Re_{pk}^{\frac{1}{2}} \quad (23)$$

The term h_{pk} is the convective heat-transfer coefficient between the kth particulate phase and the surrounding gas, and Nu_{pk} is the Nusselt number defined as the ratio of $d_{pk}h_{pk}$ to the particulate phase thermal conductivity. The fourth term on the right-hand side of Eq. (4) is the total work done on the particulate phase by the surrounding gas, causing a thermal energy loss for the gaseous phase. The last two terms in the gaseous phase thermal energy equation describe the heat loss due to mass transfer by vaporization (or gain due to condensation) process. The former is the heat needed to vaporize the particles, L_k being the latent heat of vaporization; the latter is the heat spent to raise the temperature of the vapor to that of the surrounding gas.

Equations (5) and (6) are those of the two-equation k-ϵ model of turbulent transport.[13] The model assumes that the turbulent viscosity is isotropic, and the transport equations

are solved for the kinetic energy of turbulence

$$k = \tfrac{1}{2}\overline{u_i' u_i'} \tag{24}$$

and its dissipation rate

$$\epsilon = (\partial u_i'/\partial x_j)^2 \tag{25}$$

The turbulent viscosity is calculated from the relation

$$\mu_t = C_\mu \rho_g k^2/\epsilon \tag{26}$$

whereas the effective viscosity is defined by

$$\mu_g = \mu_l + \mu_t \tag{27}$$

μ_l being the laminar viscosity of the gaseous phase. The turbulence correlations are related to μ_t by the Boussinesq relations

$$\rho_g \widetilde{\tilde{u}_i \tilde{u}_j} = -\mu_t \left(\frac{\partial \tilde{u}_i}{\partial x_j} + \frac{\partial \tilde{u}_j}{\partial x_i} - \frac{2}{3} \frac{\partial \tilde{u}_k}{\partial x_k} \delta_{ij} \right) \tag{28}$$

and

$$\rho_g \widetilde{\tilde{u}_i' \tilde{\phi}'} = \frac{\mu_t}{\sigma_\phi} \frac{\partial \tilde{\phi}}{\partial x_i} \tag{29}$$

Appearing in the diffusion terms of Eqs. (5) and (6), σ_k and σ_ϵ are the turbulent Schmidt numbers for turbulence kinetic energy and its dissipation rate, respectively. The remaining source terms are defined as

$$\dot{S}_k = G - C_D \rho_g \epsilon \tag{30}$$

and

$$\dot{S}_\epsilon = C_1 \frac{\epsilon}{k} G - C_2 \rho_g \frac{\epsilon^2}{k} \tag{31}$$

where

$$G = \mu_t \frac{\partial \tilde{u}_i}{\partial x_j} \left(\frac{\partial \tilde{u}_i}{\partial x_j} + \frac{\partial \tilde{u}_j}{\partial x_i} \right) \tag{32}$$

The model comprises six empirical constants, common values of which are[9]

$$C_1 = 1.44, \quad C_2 = 1.92, \quad C_D = 1.00$$
$$C_\mu = 0.09, \quad \sigma_k = 1.00, \quad \sigma_\epsilon = 1.22 \tag{33}$$

Equation (7) describes the conservation of mass for the kth particulate phase; ρ_{pk} represents the phase concentration (partial density) and V_{pk} its mean velocity. The production term $\dot{S}_{pk}$ includes the interphase mass transfer to the surrounding gas as well as the mass exchange between particulate phases resulting from variations in mean particle size by condensation/vaporization and coalescence/fragmentation processes:

$$\dot{S}_{pk} = B_k \rho_{pk+1} - C_k \rho_{pk} + \frac{1}{\hat{\rho}_{pk}} \frac{V}{V_1} \sum_l \sum_m A_{klm} \rho_{pl} \rho_{pm} \tag{34}$$

The first two terms on the right-hand side of Eq. (34) set the contribution from the larger-size groups and mass loss from vaporization (or gain from condensation), respectively, and the last term includes interparticle coalescence/fragmentation contributions from all neighboring size groups l and m to the kth size group. V is the control volume, whereas V_1 stands for the volume of a monomer, a unit particle definition used in interparticle collision frequency evaluations.[37] The derivation of the functional forms of the coefficients A_{klm}, B_k, and C_k is given by Tambour.[32] It is noted that since coalescence/fragmentation processes are overall-mass-conserving within particulate phases, they do not contribute to the gaseous phase production term defined in Eq. (14).

The momentum balance for the particulate phases is formulated in Eq. (8). The term σ_{pk} is the turbulent Schmidt number for the kth particulate phase, determining its turbulent diffusion through the surrounding gas. More rigorous treatments on the turbulent dispersion of particles can be found in Hinze,[11] Picart et al.,[19] and Shih and Lumley.[25] The second and third terms on the right-hand side of the equation concerning interphase momentum exchange have their counterparts in Eq. (3). The last term represents the momentum contribution of particles leaving the higher size group as a result of the vaporization process. Interparticle coalescence/fragmentation effects on the average momentum transfer between the particulate phases, which require rigorous modeling, are not incorporated.

Equation (9) sets the particulate phase thermal energy balance. The first term on the right-hand side describes the thermal diffusion within the particle cloud, c_{Vpk} being the specific heat of the particles, σ_{pHk} the turbulent Prandtl number for the particulate phase, and T_{pk} the particle mean temperature. The second and third terms represent the interphase convective heat transfer and the latent heat of vaporization, respectively, which were referred to in Eq. (4). The last term represents the thermal energy contribution of particles leaving the higher size group because of vaporization. As in the particle phase momentum equation, coalescence/fragmentation effects on interparticle heat transfer are not considered for lack of an available model.

It is noted that, under the assumptions for the transfer processes, since the thermal energy of the particles can be changed only by interphase heat transfer, the work resulting from gaseous drag on the particles affects only the kinetic energy of the particle cloud.

Boundary Conditions

For subsonic flow conditions, the elliptic nature of the coupled conservation equations (1–9) requires the specification of boundary conditions for each dependent variable at the boundaries of the solution domain to complete the definition of the physical problem. The domain under consideration is the half-section of an axisymmetric ram combustor model. The combustor geometry and appropriate boundary conditions are illustrated in Fig. 2.

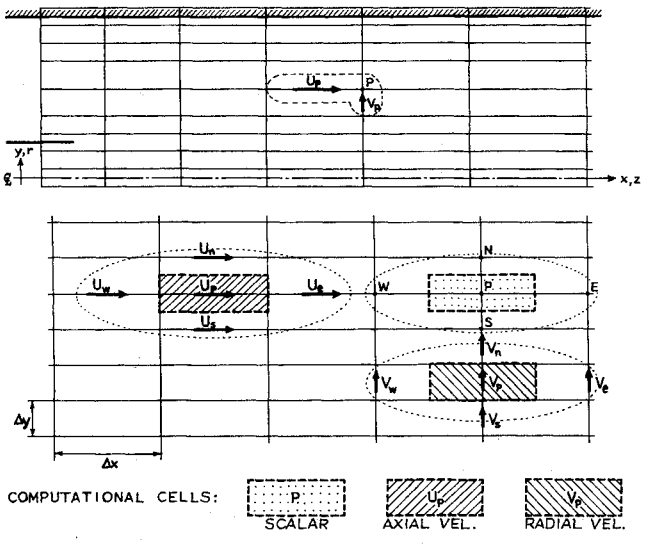

Fig. 2 Ram combustor geometry and computational grid system.

Inlet

As seen in Fig. 2, the inner and outer inlets simulate the gas generator nozzle exit and air inlet, respectively. The inclination of the outer inlet flow is denoted by α, whereas the nozzle spread angle β, for the inner inlet, can be set to describe the expansion of gas generator exhaust. Distributions of all of the dependent variables are specified at the inlet cross section.

Outlet and Symmetry Axis

The axial gradients of the dependent variables are set to zero at the outlet whereas, at the centerline, the radial gradients vanish as a result of symmetry.

Solid Boundary

To avoid the need for detailed calculations for the gaseous phase in the vicinity of the wall where the laminar and turbulent effects are of the same order of magnitude, a one-dimensional Couette flow analysis is made.[9] The layer is assumed to be one of constant shear stress and constant (or zero) heat/mass flux, which is adequate for an impervious wall, with a zero or negligible streamwise pressure gradient. The momentum equation is then reduced to a particularly simple dimensionless form:

$$\tau = (\mu_l + \mathrm{m}_t)\frac{\mathrm{d}u}{\mathrm{d}y} \quad \text{or} \quad \frac{\tau}{\tau_w} = \left(1 + \frac{\mu_t}{\mu_l}\right)\frac{\mathrm{d}u^+}{\mathrm{d}y^+} \tag{35}$$

where

$$y^+ = \frac{\rho_g u_\tau y}{\mu_g}, \qquad u^+ = \frac{u_g}{u_\tau}, \qquad u_\tau = \left(\frac{\tau_w}{\rho_g}\right)^{\frac{1}{2}} \tag{36}$$

The terms τ and y represent the shear stress and the coordinate normal to the wall, respectively, superscript + denotes a normalized quantity, and subscript w refers to the value on the wall; y^+ is identified as the local Reynolds number, with u^+ the "friction velocity."

The flow region near the wall is separated into three zones: the viscous sublayer ($0 < y^+ < 5$), where viscous effects dominate; the inertial sublayer ($30 < y^+ < 400$), where the flow is assumed completely turbulent; and the transition zone ($5 < y^+ < 30$). The conventional approach is to dispose this transition zone by defining a point $y^+ = 11.63$, below which the flow is assumed purely laminar and above which it is purely turbulent:

$$\text{For } y^+ \le 11.63\, u^+ = y^+, \quad \text{otherwise } u^+ = 1/\kappa ln\,(Ey^+) \tag{37}$$

where

$$\mu_t = \kappa \rho_g y u_\tau, \qquad \kappa = 0.4187, \qquad E = 9.793 \tag{38}$$

κ represents the von Kármán constant, and E is an integration constant depending on the magnitude of the variation of shear stress across the layer and on the wall roughness.[9] The same treatment goes for heat or any other scalar transport as the momentum transport.

As for the particulate phase, no boundary-layer assumptions are made in the vicinity of the wall. The fluxes of all particulate phase variables are merely set to zero on the solid boundaries.

Solution Method

TEACH-T Code

The present study utilizes the SIMPLE (semi-implicit method for pressure-linked equations) procedure developed by Patankar and Spalding,[17] available as the TEACH-T code,[9] for the numerical solution of the equations system described in the previous section. The governing equations were reformulated into conservative form so that the SIMPLE procedure could be appropriately implemented.

The general form of the equations describing two-dimensional flows is partial differential in form and elliptic in nature:

$$\frac{\partial}{\partial z}(\rho u\phi) + \frac{1}{r}\frac{\partial}{\partial r}(\rho r v\phi) = S^\phi + \frac{\partial}{\partial z}\left(\Gamma_\phi \frac{\partial \phi}{\partial z}\right) + \frac{1}{r}\left(\Gamma_\phi r \frac{\partial \phi}{\partial r}\right) \tag{39}$$

In this equation, u and v represent the time-averaged velocities in the axial and radial directions, respectively. The variable ϕ stands for time-averaged quantities, such as mean velocities, turbulence kinetic energy, turbulence energy dissipation rate. The transport coefficient Γ_ϕ assumes its proper representation for each variable ϕ. S^ϕ stands for source term contribution, such as generation/destruction, pressure and body forces. For $\phi = 1$ and $\Gamma_\phi = S^\phi = 0$, Eq. (39) transforms into the continuity equation.

A typical computational grid system used in the present study is shown in Fig. 2. This rectangular grid pattern is laid out on the physical domain of interest. A nonuniform grid, with finer spacings in the regions where large spatial gradients prevail, is generally preferable. Each computational cell (control volume) surrounds the point of location of the relevant variable. Staggered control volumes are used for the axial and radial velocity components, as indicated in Fig. 2. The remaining scalar quantities of interest are computed at the grid nodes. Hence, the storage locations of the velocities and scalar variables pertaining to each node form a triad, as emphasized in the same figure by dotted lines within the grid. This staggered system has the advantage that the variables U, V, P are stored such that the pressure gradients driving the velocities are easy to evaluate. Moreover, the velocity locations readily facilitate the calculation of convective fluxes.

The finite-difference form of the time-averaged equations can be obtained through a semi-integral approach to discretize the equations over each computational cell of the grid. The resulting set of simultaneous, nonlinear algebraic equations are solved by an iterative line-by-line procedure.[9]

Modified Version of TEACH-T

The rather versatile and modular structure of the original TEACH-T code allowed the accommodation of particulate phase equations and the incorporation of mutual interactions between the phases.

Equations (1–9), describing the multiphase flowfield, are included in their complete form in the structure of the modified version. Out of those, the newly introduced equations are: 1) the gaseous phase specie equation (2), 2) the particulate phase continuity equation (7), 3) the particulate phase momentum equation (8), 4) the particulate phase thermal energy equation (9). The specie Eq. (2) was added to gaseous phase equations to account for the second component besides air; CO_2 for cold-flow simulation, and fuel-rich gas generator exhaust for hot-flow simulation.

Since the particulate phase equations match the general form of Eq. (39), their incorporation did not pose significant problems. The particulate phase concentration Eq. (7) is treated like that of any other scalar variable, whereas the momentum Eq. (8) and thermal energy Eq. (9) both have their counterparts in the gaseous phase equations. The differences are in the values of the transport coefficients and in the additional source terms due to interaction between the phases. All of the particulate phase equations are divided into subphases (size groups) within themselves, enabling simultaneous treatment of particles of up to five different sizes.

In order to attain reasonable convergence characteristics for a system of strongly coupled nonlinear equations, a special iteration procedure is employed, as outlined in the following.

In the beginning, iterations for the gaseous phase equations are performed. Once the desired convergence is obtained, the iteration process is switched to the particulate phase equa-

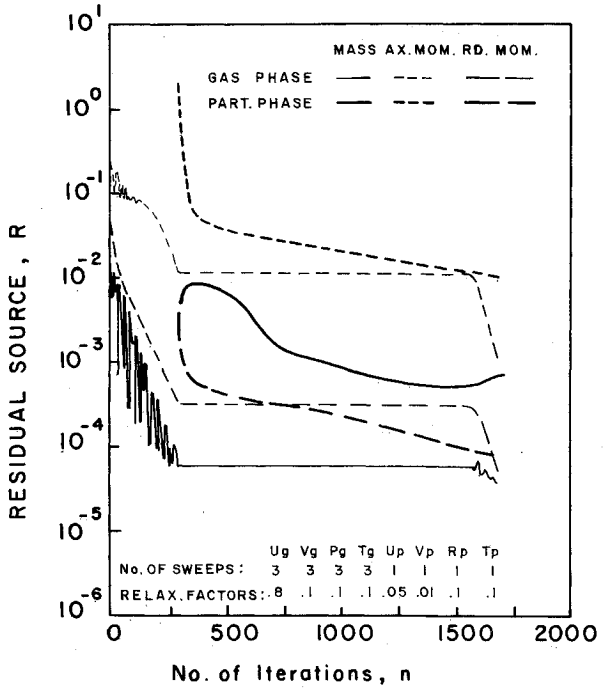

Fig. 3 Convergence characteristics of case 1.

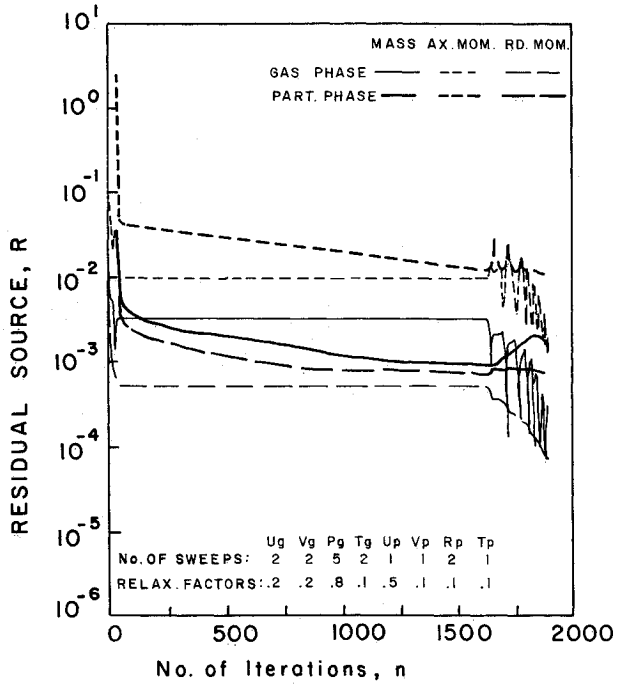

Fig. 4 Convergence characteristics of case 1 for a different choice of relaxation factors.

tions, leaving the previously converged gas field idle. After the convergence of particulate phase equations, the entire set of equations, including the interaction terms, are solved until the desired accuracy is obtained for each equation. If a tendency of divergence in the solution of one (or more) of the equations corresponding to a certain phase is detected, the pertinent relaxation factors are adjusted (in most cases, decreased), and the equations of the other phase are temporarily abandoned to secure the overall convergence.

Figures 3–5 illustrate the convergence characteristics of the two numerical simulations that will be described in the next section. The fluctuations in the residual sources for the

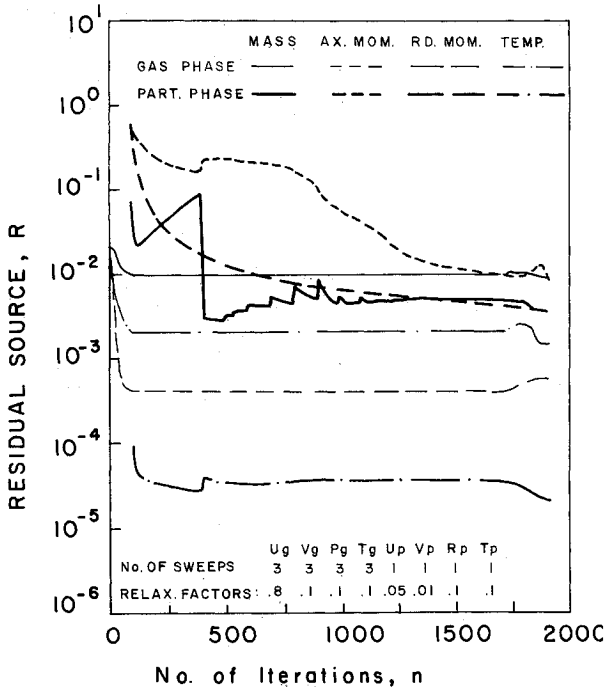

Fig. 5 Convergence characteristics of case 2.

gaseous phase, shown in Fig. 3 (Case 1 simulation), result from the improper specification of the initial field guess. Particulate phase convergence exhibits a slow but persistent character, until simultaneous iterations take over and both of the fields converge in relatively few iterations. A different convergence pattern for the same simulation is given in Fig. 4, where the input of a previously converged field, as an initial guess, has accelerated the gas phase convergence. From comparison of the last stages of convergence in Figs. 3 and 4, it can be deduced that the underrelaxation factor employed in the particulate phase axial momentum equation has a crucial role in promoting stability. The optimal value of this factor for the case under investigation was 0.3, with an upper limit of 0.6.

Figure 5 shows the convergence history of the hot-flow simulation, Case 2. Especially low underrelaxation factors were employed in particulate phase momentum equations at preliminary stages of the iterations. These factors were then gradually increased after every 100 iterations up to their conventional values.

The computational grid was selected following a resolution study on successively finer grids and taking into consideration the memory and run time restrictions. An axially stretched 42×42 orthogonal grid pattern was found to be satisfactory. Every iteration step toward the solution of the coupled equations required ~ 3 s of CPU time at an IBM 3081D computer whereas, in all cases studied, fewer than 2000 iterations were sufficient to satisfy the total residual source criterion of 10^{-2}. This criterion compares the sum of the residues of the finite-difference equations solved for each cell to the relevant extensive property flux fed into the calculation domain.[9]

Ram Combustor Simulations

Two numerical simulations, named Case I (cold flow) and Case 2 (hot flow) were performed during this study. The main parameters of these simulations are summarized in Table 1.

Simulation Case 1

This simulation was planned as a preliminary study in order to test the adequacy of the physical model employed through comparison with experimental results. The geometry and flow

Table 1 Simulation parameters of cases 1 and 2

Parameter	Case 1	Case 2
Geometry		
Combustor length, L	1.430 m	1.430 m
Combustor diameter, d_{out}	0.103 m	0.103 m
Primary inlet diameter, d_{in}	0.014 m	0.014 m
Secondary inlet slope, α	0 deg	−15 deg
Primary inlet		
Gas velocity, V_g	42.5 m/s	750 m/s
Mach number, M	0.12	0.92
Gas temperature, T_g	300 K	1800 K
Gas density, ρ_g	1.24 kg/m^3	1.06 kg/m^3
Specie mass fraction, Y_i	0.10	1.00
Specie molecular weight, W_i	44.0 kg/kg-mole	26.0 kg/kg-mole
Turbulence kinetic energy, k	27.1 m^2/s^2	1.7×10^4 m^2/s^2
Particle velocity, V_p	41.4 m/s	675 m/s
Particle temperature, T_p	300 K	1500 K
Particle concentration, ρ_p	0.01 kg/m^3	0.01 kg/m^3
Particle absolute density, $\hat{\rho}_p$	4×10^3 kg/m^3	4×10^3 kg/m^3
Particle mean diameter, d_p	20 μm	20 μm
Secondary inlet		
Gas velocity, V_g	22.5 m/s	250 m/s
Mach number, M	0.06	0.53
Gas temperature, T_g	300 K	600 K
Gas density, ρ_g	1.18 kg/m^3	3.53 kg/m^3
Turbulence kinetic energy, k	7.6 m^2/s^2	1.9×10^3 m^2/s^2
Outlet		
Pressure, P	10^5 Pa	6×10^5 Pa
Average Reynolds no., $\overline{Re}$	1.4×10^5	9.8×10^5
Duct wall	Adiabatic Impervious	Adiabatic Impervious

conditions were identical to those of the experimental facility, as described in our TAE report 627.[1]

The case in consideration was the isothermal (300 K) flow of confined, concentric two-phase jets. Particles introduced by the primary (inner) jet, with a slight initial velocity lag, were assumed to have a uniform diameter of 20 μm (see Table 1). The particulate phase Schmidt number in Eq. (8) was taken as unity. The tracer gas (CO_2) mass fraction in the primary flow was 0.10. The resulting primary-to-secondary mass flow ratio and momentum ratio were 0.035 and 0.066, respectively.

Simulation Case 2

After verification of the previous simulation by experimental results, a more realistic ram combustor simulation was performed. The ram rocket was assumed to fly at sea level at a Mach number of 2.3 with a normal shock at the ram inlet, revealing a heating ratio of ~2 and a compression ratio of ~6. The inclination of the secondary airflow at the combustor inlet was $\alpha = 15$ deg (see again Fig. 2). The gas generator exhaust was treated as a single component gas of 26 kg/kg-mole, containing inert particles of 20-μm diameter. The par-

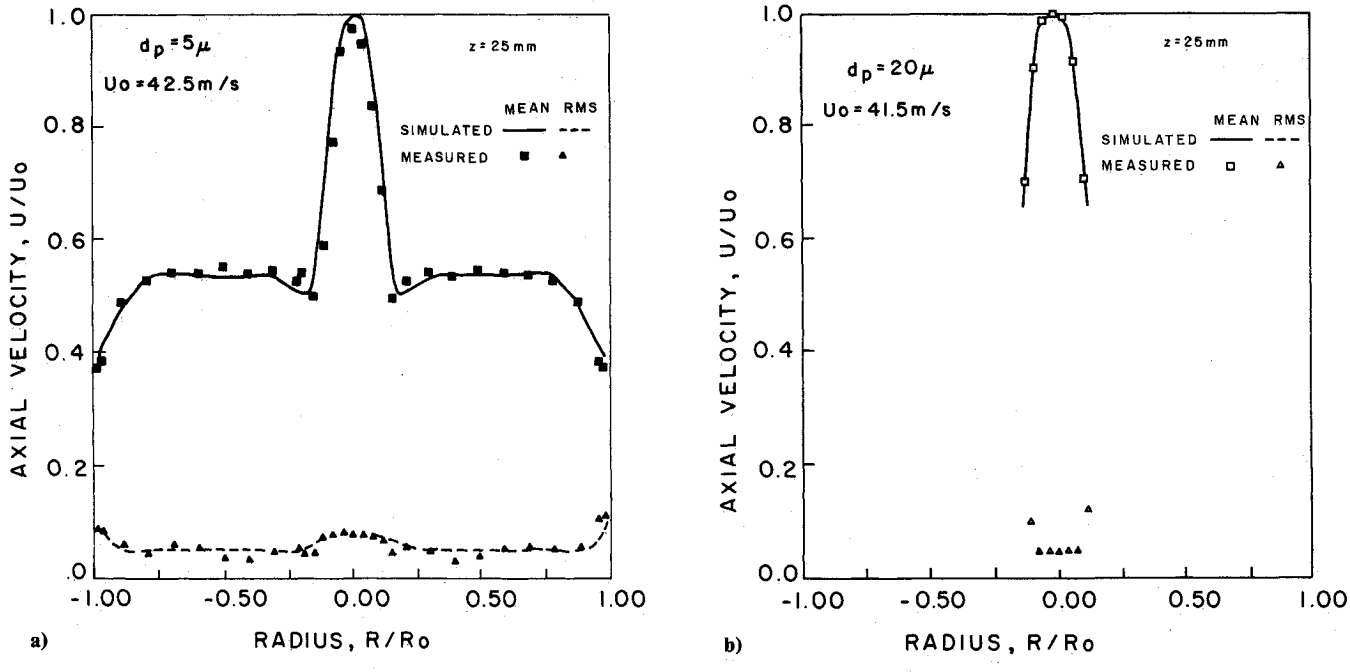

Fig. 6 Measured a) gas and b) particle velocity profiles at the inlet cross section, taken as initial conditions for simulation case 1.

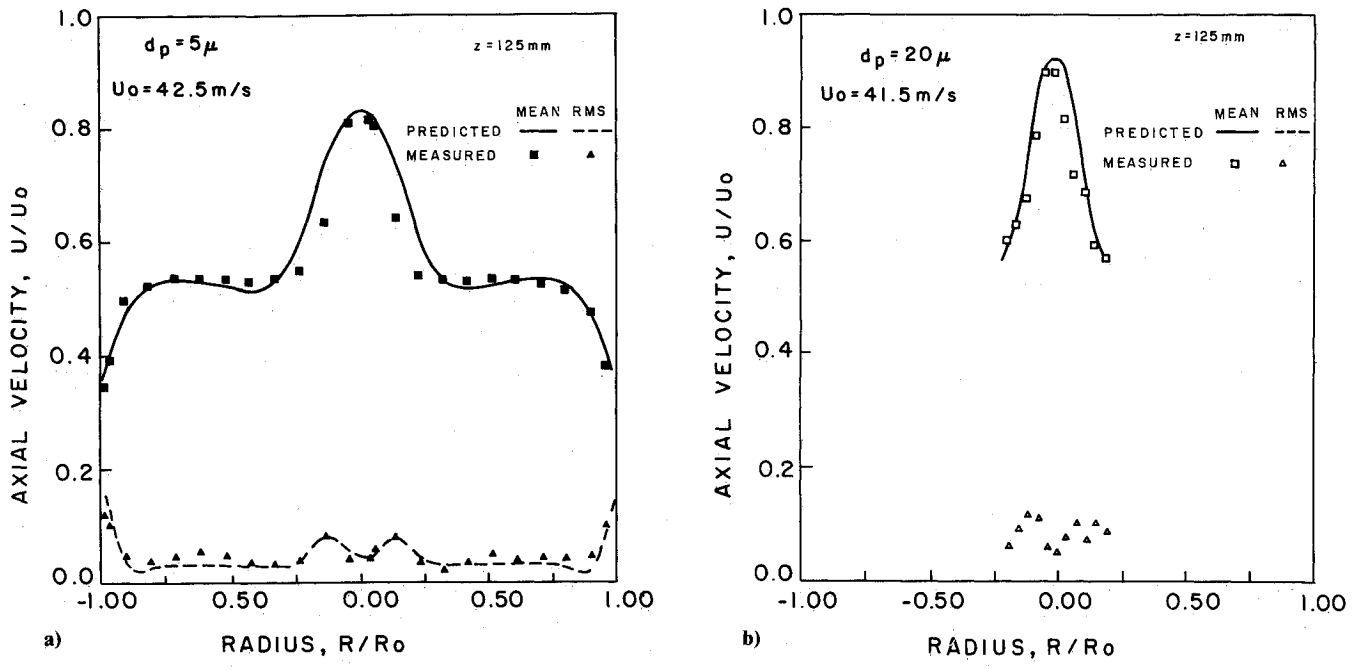

Fig. 7 Measured vs predicted a) gas and b) particle velocity profiles 100 mm downstream from the inlet plane (case 1).

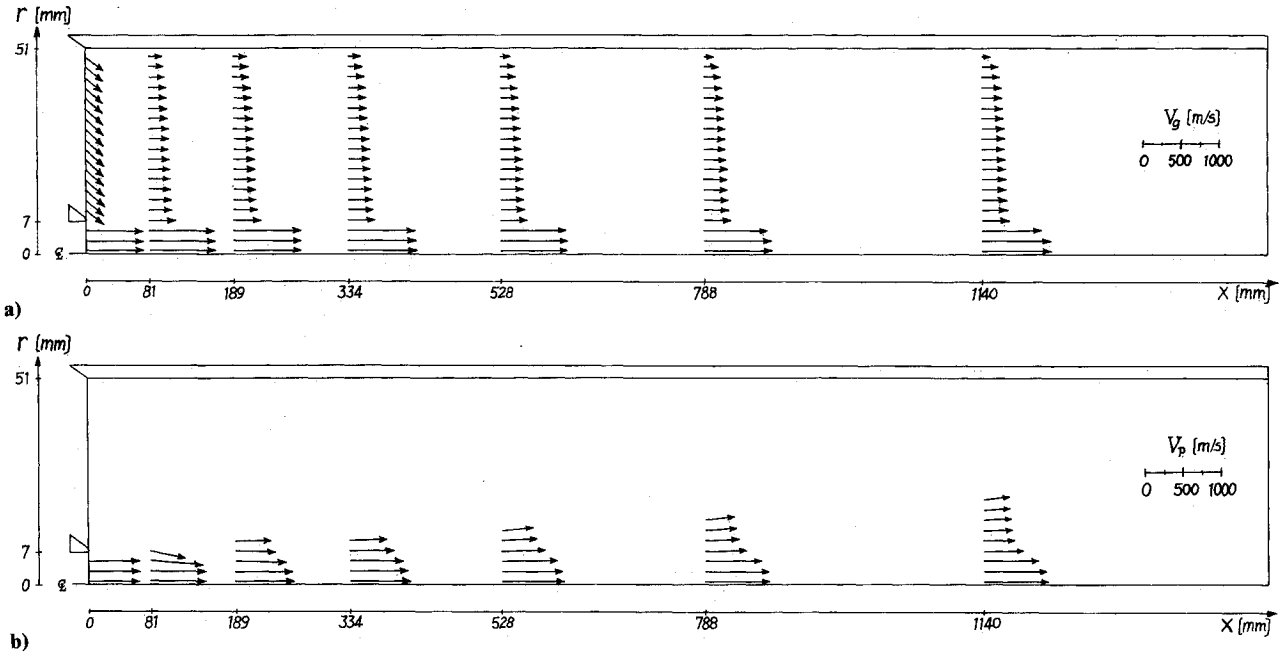

Fig. 8 Predicted a) gas and b) particle velocity fields (case 1).

ticulate phase Schmidt number was again taken as unity. The Mach number of the primary flow was 0.92 and the gas temperature 1800 K. A velocity, as well as a temperature lag, was imposed on the particles (see Table 1). The primary-to-secondary mass flow ratio and momentum ratio were 0.019 and 0.060, respectively.

Computational Results and Discussion

Graphic representations of the calculated flowfields referring to the simulation cases 1 and 2 are given in Figs. 6–10. For clarity, the scale of the ordinates in Figs. 8–10 has been taken five times as great as that of the abscissas.

Case 1

Measured gas and particle phase velocity profiles in the inlet plane of the combustor are shown in Figs. 6a and 6b, respectively.[1] Smoothed profiles taken as initial conditions for the numerical simulation are also shown in these figures. Figures 7a and 7b show the evolution of the velocity profiles 100 mm downstream from the inlet plane. A satisfactory quantitative agreement can be observed between predicted and measured mean velocity values for both phases, with discrepancies less than 2% at the central zone and slightly larger elsewhere. The width of the inner jet wake was somewhat overestimated, which is characteristic to the adopted turbulence model. The turbulence intensity predictions are very accurate. This is especially emphasized at central double peak and near-wall distributions, in location as well as in magnitude. Achieving such an agreement between predicted and measured values is quite unique and also indicates the accuracy of the LDV measurements.[1]

As for the particulate phase, a very good matching is seen

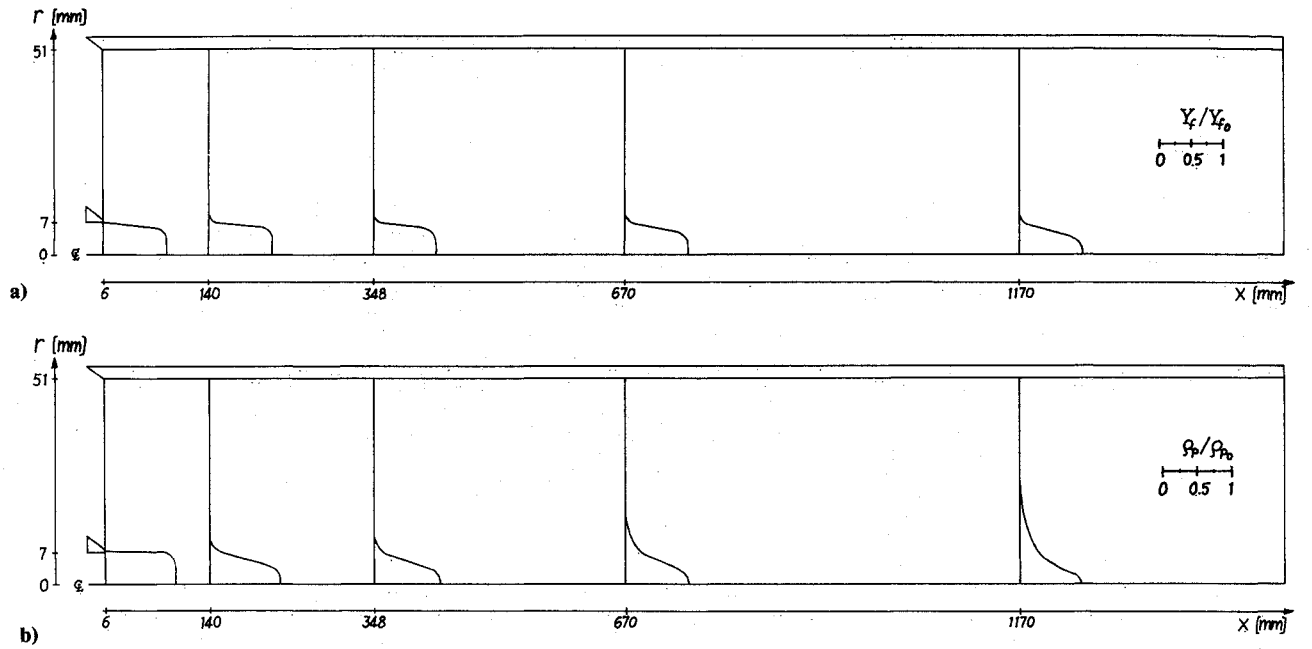

Fig. 9 Predicted a) primary exhaust and b) particle concentration profiles (case 2).

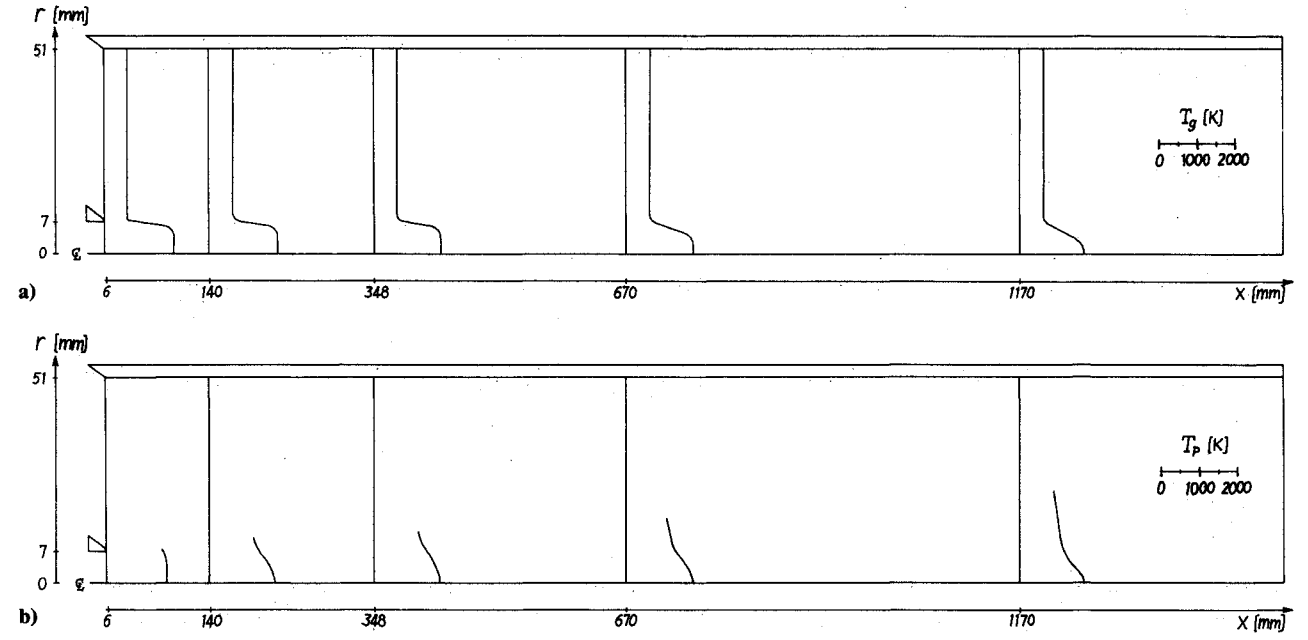

Fig. 10 Predicted a) gas and b) particle temperature profiles (case 2).

between the predicted and measured mean velocity distribution, with differences lower than 2% anywhere. The predicted and measured jet widths are almost identical. No comparison could be made for the turbulence intensity distribution because of the lack of an appropriate model.

Case 2

Vector plots of gas and particle phase velocity fields are shown in Figs. 8a and 8b, respectively. Fuel-rich gas generator exhaust mass fraction and particle concentration profiles are given in Figs. 9a and 9b, whereas gas and particle temperature profiles are shown in Figs. 10a and 10b, respectively. The mass fraction and temperature profiles of gas generator exhaust gases display like behavior, as expected, since the mechanism of mass and thermal energy transfer are similar in the physical model.

It is noted that the particulate phase velocity and temperature profiles should be analyzed in coordination with the corresponding concentration field, inasmuch as these values lose their significance in regions where the particle concentration tends to vanish.

As can be seen in Fig. 8a, the gas phase flowfield exhibits an intense stratification, starting from the gas generator nozzle lip, suppressing the turbulent mixing of primary and secondary streams. Although discouraging at first sight, this may be favorable for the auto-ignition process, which necessitates the control of excessive mixing right after the primary nozzle expansion.

Nonparallel injection of the secondary ram air does not reveal a large recirculation zone needed for flame stabilization, probably because of its high axial momentum and flow rate. The limited resolution of the computational grid for detection of minor domains with backflow might have also contributed to this situation. It seems that a satisfactory

recirculation can only be achieved by means of abrupt expansion under such flow conditions.

Conclusions

A physical model describing the two-phase flowfield in ram combustors is developed and validated by numerical simulations for simple combustor geometries. Although the investigated configuration does not reveal an efficient ram combustor with plausible mixing characteristics, the computer code developed during this study has proved a useful tool for the optimization of geometry and flow patterns toward a better design of ram combustors. The model can be further enhanced by the incorporation of chemical reactions, radiative heat transfer, and two-phase turbulence modeling, all of which are beyond the scope of the present study.

References

[1]Albagli, D. and Levy, Y., "Two-Phase Flow Measurements in Confined Coaxial Jets," Technion, Haifa, Technion Aerospace Engineering Rept. 627, 1988.

[2]Bird, R. B., Stewart, W. E., and Lightfoot, E. N., *Transport Phenomena*, Wiley, New York, 1960.

[3]Chigier, N. A. and Beér, J. M., "The Flow Region Near the Nozzle in Double Concentric Jets," *Journal of Basic Engineering (Transactions of ASME)*, Dec. 1964, pp. 797–804.

[4]Choudhury, P. R., "Characteristics of a Side Dump Gas Generator Ramjet," AIAA Paper 82-1258, June 1982.

[5]Curtet, R., "Confined Jets and Recirculation Phenomena with Cold Air," *Combustion and Flame*, Vol. 2, 1958, pp. 383–411.

[6]DiGiacinto, M., Sabetta, F., and Piva, R., "Two-Way Coupling Effects in Dilute Gas-Particle Flows," *Journal of Fluids Engineering (Transactions of ASME)*, Vol. 104, Sept. 1982, pp. 304–312.

[7]Genovese, J., Edelman, R. B., and Fortune, O. F., "Some Aspects of Two-Phase Flows with Mixing and Combustion in Bounded and Unbounded Flows," *Journal of Spacecraft*, Vol. 8, April 1971, pp. 352–357.

[8]Ghia, K. N., Torda, T. P., and Lavan, Z., "Turbulent Mixing in the Initial Region of Heterogeneous Axisymmetric Coaxial Confined Jets," NASA CR-1615, May 1970.

[9]Gosman, A. D. and Ideriah, F. J. K., "TEACH-T: A General Computer Program for Two-Dimensional, Turbulent, Recirculating Flows," Imperial College, London, Mechanical Engineering Dept. Rept., June 1976.

[10]Gutmark, E. and Schadow, K. C., "Behavior of Elliptic Jets in a Gas Generator Ramjet Environment," *Proceedings of the 27th Israel Annual Conference on Aviation and Astronautics*, Technion, Haifa, Israel, Feb. 1985.

[11]Hinze, J. O., "Turbulent Fluid and Particle Interaction," *Progress in Heat and Mass Transfer*, Vol. 6, 1971, pp. 433–452.

[12]Ishikawa, N., "Experimental Study of Jet Mixing Mechanisms in a Model Secondary Combustor," *AIAA Journal*, Vol. 21, April 1983, pp. 565–570.

[13]Jones, W. P. and Launder, B. E., "The Prediction of Laminarization with a Two-Equation Model of Turbulence," *International Journal of Heat and Mass Transfer*, Vol. 15, No. 2, Feb. 1972, pp. 301–314.

[14]Knudsen, J. G. and Katz, D. L., *Fluid Dynamics and Heat Transfer*, McGraw-Hill, New York, 1958.

[15]Migdal, D. and Agosta, V. D., "A Source Model for Continuum Gas-Particle Flow," *Journal of Applied Mechanics (Transactions of ASME)*, Dec. 1967, pp. 860–865.

[16]Miller, W., McClendon, S., and Burkes, W., "Design Approaches for Variable Flow Ducted Rockets," AIAA Paper 81-1489, July 1981.

[17]Patankar, S. V. and Spalding, D. B., "A Calculation Procedure for Heat, Mass, and Momentum Transfer in Three-Dimensional Parabolic Flows," *International Journal of Heat and Mass Transfer*, Vol. 15, No. 10, Oct. 1972, pp. 1787–1806.

[18]Peters, C. E., Phares, W. J., and Cunningham, T. H. M., "Theoretical and Experimental Studies of Ducted Mixing and Burning of Coaxial Streams," *Journal of Spacecraft*, Vol. 6, Dec. 1969, pp. 1435–1441.

[19]Picart, A., Berlemont, A., and Gouesbet, G., "Modeling and Predicting Turbulence Fields and the Dispersion of Discrete Particles Transported by Turbulent Flows," *International Journal of Multiphase Flow*, Vol. 12, No. 2, 1986, pp. 237–261.

[20]Razinsky, E. and Brighton, J. A., "A Theoretical Model for Nonseparated Mixing of a Confined Jet," *Journal of Basic Engineering (Transactions of ASME)*, Sept. 1972, pp. 551–558.

[21]Schadow, K. C., "Boron Combustion Characteristics in Ducted Rockets," *Combustion Science and Technology*, Vol. 5, 1972, pp. 107–117.

[22]Schadow, K. C., "Study of Gas Phase Reactions in Particle Laden, Ducted Flows," *AIAA Journal*, Vol. 11, July 1973, pp. 1042–1044.

[23]Schadow, K. C., "Fuel-Rich, Particle Laden Plume Combustion," AIAA Paper 75-245, Jan. 1975.

[24]Schadow, K. C., Lee, M. C., and Wilson, K. J., "Turbulent Mixing and Combustion of Multi-Phase Reacting Flows in Ramjet and Ducted Rocket Environment," Annual Rept. April 1980–Sept. 1981, Naval Weapons Center, China Lake, CA, AFOSR-TR-82-0150, March 1982.

[25]Shih, T. H. and Lumley, J. L., "Second Order Modeling of Particle Dispersion in a Turbulent Flow," *Journal of Fluid Mechanics*, Vol. 163, 1986, pp. 349–363.

[26]Smoot, L. D. and Anderson, G. S., "Boron Particle Nonequilibrium Effects in Combusting Ducted Flows," *AIAA Journal*, Vol. 10, July 1972, pp. 857–858.

[27]Smoot, L. D. and Fort, L. A., "Confined Jet Mixing with Nonparallel Multiple-Port Injection," *AIAA Journal*, Vol. 14, April 1976, pp. 419–420.

[28]Soo, S. L., *Fluid Dynamics of Multiphase Systems*, Blaisdell, Waltham, MA, 1967, pp. 259–261.

[29]Streby, G. D., "Multi-Ducted Inlet Combustor Research and Development," Interim Rept. Sept. 1982–Aug. 1983, Aero Propulsion Laboratory, Wright-Patterson AFB, OH, AFWAL-TR-83-2081, Nov. 1983.

[30]Stull, F. D., Craig, R. R., Streby, G. D., and Vanka, S. P., "Investigation of a Dual Inlet Side Dump Combustor Using Liquid Fuel Injection," *Journal of Propulsion*, Vol. 1, Jan.–Feb. 1985, pp. 83–88.

[31]Sykes, R. I., Lewellen, W. S., and Parker, S. F., "A Turbulent Transport Model for Concentration Fluctuations and Fluxes," *Journal of Fluid Mechanics*, Vol. 139, Feb. 1984, pp. 193–218.

[32]Tambour, Y., "A Sectional Model for Evaporation and Combustion of Sprays of Liquid Fuels," *Israel Journal of Technology*, Vol. 18, 1980, pp. 47–56.

[33]Tsujikado, N., "An Experimental Study on Configuration of Secondary Combustor Chamber for Ram Rocket," *6th International Symposium on Air Breathing Engines, Symposium Papers*, AIAA, New York, June 1983, pp. 3–8.

[34]Tufts, L. W. and Smoot, L. D., "A Turbulent Mixing Coefficient Correlation for Coaxial Jets with and without Secondary Flows," *Journal of Spacecraft*, Vol. 8, Dec. 1971, pp. 1183–1190.

[35]Wallis, G. B., *One-Dimensional Two-Phase Flow*, McGraw-Hill, New York, 1969, p. 178.

[36]Williams, A., "Combustion of Droplets of Liquid Fuels: A Review," *Combustion and Flame*, Vol. 21, Aug. 1973, pp. 1–31.

[37]Yuu, S., "Collision Rate of Small Particles in a Homogeneous and Isotropic Turbulence," *AIChE Journal*, Vol. 30, No. 5, 1984, pp. 802–807.

[38]Zetterström, K. A., Sjöblom, B., and Jarnmo, A., "Solid Ducted Rocket Engine Combustor Tests," *6th International Symposium on Air Breathing Engines, Symposium Papers*, AIAA, New York, June 1983, pp. 9–16.